Spring 5-3-2019

Synthesis of Piperidine-Based Inhibitors of KasA, a Vital Enzyme of M. tuberculosis

Lindsey Jones

Title: Synthesis of Piperidine-Based Inhibitors of KasA, a Vital Enzyme of *M. tuberculosis*

Name of Candidate: Lindsey Jones

Approved by Examination Committee:

Edward Davis Oldham

Dr. E. Davis Oldham
Assistant Professor of Chemistry

Janet A. Asper PhD.

Dr. Janet A. Asper
Professor of Chemistry

K. Nicole Crowder

Dr. K. Nicole Crowder
Associate Professor of Chemistry

Randall D. Reif

Dr. Randall D. Reif
Assistant Professor of Chemistry

Date Approved: 9/3/2019

Synthesis of Piperidine-Based Inhibitors of KasA, a Vital Enzyme of *M. tuberculosis*

Lindsey Jones

Thesis submitted to the faculty of the University of Mary Washington in partial fulfillment of the requirements for graduation with Honors in Chemistry

(2019)

Abstract

Tuberculosis is the leading cause of death from infectious disease in the world. Although tuberculosis drugs exist, the rise of drug-resistant tuberculosis has created a need for new research. Identifying novel, effective drugs for treatment of tuberculosis could reduce the cost of care and treatment time, saving millions of lives. The enzyme KasA, which synthesizes part of the tuberculosis bacterial cell wall, has been identified as an attractive drug target. A virtual screen using KasA discovered a compound, 4-(4-bromophenyl)-1-pyrenemethyl-4-piperidinol (1), which inhibited bacterial growth *in vitro*. In this research, nine derivatives of compound 1 were synthesized for future testing with live bacteria. A lithium-halogen exchange reaction was used to attempt to create a piperidinone-based derivative with varied substituents, but the method yields were low and difficult to purify. A Grignard process was also attempted with similar results. Alkylation of 4-substituted-4-piperidinols was successful in creating derivatives with arylmethyl substituents in yields from 51-85%. A silane reduction to remove the 4-hydroxy group was also explored but exhibited low yields. In future research, these derivatives will be tested *in vitro* to determine suitability for development as potential tuberculosis drugs.

Acknowledgements

As my part in this project comes to a close, I find I have many people to acknowledge. First, I have to thank Dr. Janet Asper, who encouraged me to participate in the UMW Summer Science Institute in 2017 and told me matter-of-factly after taking her organic class that I should plan to do an Honors project my senior year. She introduced me to Dr. Davis Oldham, my research advisor, who I have worked with on this project for the past two years. I am so grateful for both his guidance and also the independence I've been given to learn, practice new techniques, and most of all to make mistakes throughout my research experience. It has been my great fortune to work on this project in the supportive environment provided by the entire UMW chemistry faculty and student body.

Without the financial support of the UMW Summer Science Institute, UMW Undergraduate Research Grants, and the Bernard L. Mahoney Research Fellowship this research and my presentation opportunities at SERMACS in Charlotte, NC and the ACS national conference in Orlando, FL would not have been possible.

Finally, I would like to thank my fiancé Jon, whose support has been unwavering for these past three years of lab reports, presentations, and exams.

Table of Contents

List of Figures

List of Schemes

I. Introduction

Tuberculosis (TB) is the worldwide leading cause of death from infectious disease. In 2016, there were six million new cases of TB, and although the death rate has decreased by an average of 3% per year since 2000, 16% of cases still result in death.[1] In the same year, multi-drug resistant tuberculosis (MDR-TB), resistant to front-line drugs such as rifampin and isoniazid,[2] was discovered in 490,000 cases.[1] Treatment success for MDR-TB is just 54%, and the need for novel chemotherapeutics is rising.[1]

TB is a disease of the lungs caused by *Mycobacterium tuberculosis*, a member of a family of bacteria characterized by thick, waxy cell walls. These cell walls are made up of numerous long-chain fatty acids called mycolic acid, shown in Figure 1.[3] Their structure consists of two branches: the longer meromycolate chain and a shorter saturated chain. The fatty acid synthase II (FAS II) group of enzymes is responsible for the metabolic pathway generating the meromycolate chain, shown in Figure 2A. Multiple FAS II enzymes have been targeted for development as drugs for the treatment of MDR-TB.[2]

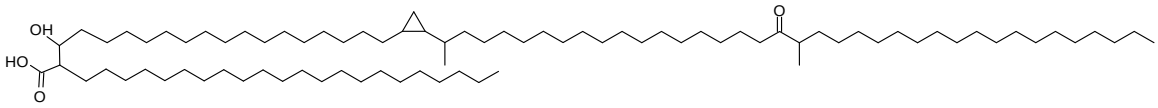

Figure 1: A mycolic acid, a characteristic long fatty acid that makes up part of the cell wall of *m. tuberculosis*. As part of the FAS II condensing system, KasA is responsible for the elongation of the top chain, called the meromycolate backbone.

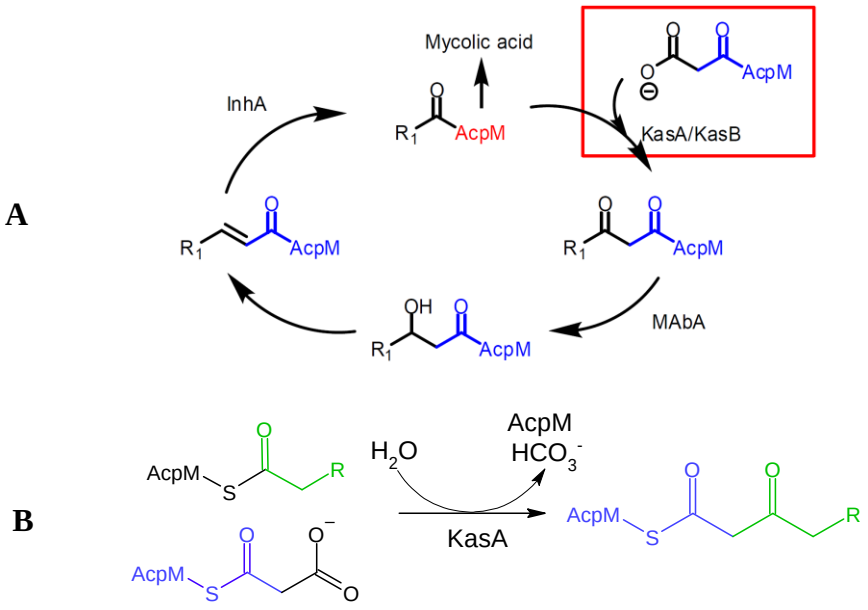

Figure 2: **A.** A diagram of the FAS II metabolic pathway, with KasA and its substrate boxed. The R_1 group is the lengthening meromycolate chain.[4] **B.** A detail of the reaction catalyzed by KasA, where AcpM is an acyl group carrier protein that shuttles growing chains throughout the FAS II system. KasA lengthens the meromycolate chain by one carbon on each catalytic cycle.

The FAS II pathway consists of enzymes which form and elongate the long-chained fatty acid, a critical contributor to the unique cell wall structure of mycobacteria.[3,5] Inhibitors like isoniazid and triclosan have been developed for the FAS II enzyme InhA,[6] and thiolactomycin and platensimycin target KasA and KasB.[7–9] KasA, also called β-ketoacyl-acyl carrier protein synthase I, is an attractive drug target because its inhibition leads to bacterial cell death.[10]

The KasA enzyme is responsible for catalyzing a Claisen condensation that creates a β-keto ester, the result of a carbon-carbon bond between an ester and carbonyl, shown in Figure 2B.[4] This reaction is necessary for the early growth of the long chain fatty acids which become mycolic acid.[11] The structure of KasA, shown in Figure3, is homodimeric, made of two symmetrical lobes which can partially open in a scissoring

motion to accommodate long hydrophobic chains, funneling the substrate to the active site near the center of the enzyme.[12]

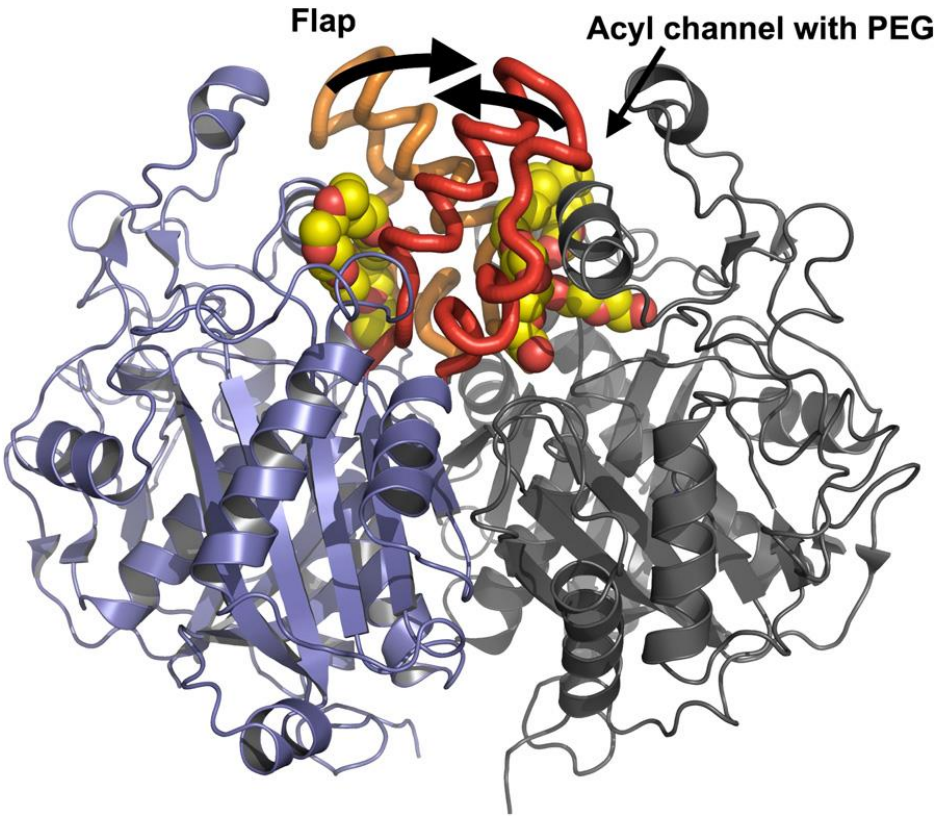

Figure 3: The crystal structure and enzyme opening proposed by Luckner et al. shows the two lobes of KasA in gray and blue, and the flexible opening of the enzyme in orange and red ribbons. Shown in red and yellow spheres are polyethylene glycol chains filling the hydrophobic acyl channels.[12]

With the advent of powerful bioinformatic tools, new drugs can be discovered via virtual enzyme-ligand modeling[13], and many new potential drug targets have been discovered by virtual screen.[14,15] An effective competitive inhibitor of KasA would prevent the enzyme from binding its typical substrate. This would prevent the elongation of the meromycolate backbone and the formation of the critical mycolic fatty acids that make up the mycobacterial cell wall, killing the bacteria. A KasA inhibitor could become a potential drug for treatment of MDR-TB.

In previous work by this group, around four million unique compounds were modeled in the active site of KasA using AutoDock Vina. The compounds were tested for their dissociation constant (pK_d) from the KasA active site, with the largest pK_d indicating the greatest inhibitory effect. Of the compounds screened, six commercially available compounds were chosen due to their predicted pK_d values, which ranged between 12.7 and 13.1. These high pKd indicate that very few inhibitor molecules would be dissociated from the enzyme at equilibrium. These were purchased and tested on *Mycobacterium bovis*, a nonpathogenic bacterium similar to *M. tuberculosis.* The results of this test are shown in Figure 4. The top three plates are a control and two compounds which had no effect on *M. bovis*. In the bottom three wells, 4-(4-bromophenyl)-1-pyrenemethyl-4-piperidinol (**1**) is shown tested in concentrations of 50, 5, and 0.5 µM. Of the tested compounds, **1** was shown to inhibit bacterial growth at a concentration of 5 µM, promising for future drug development.

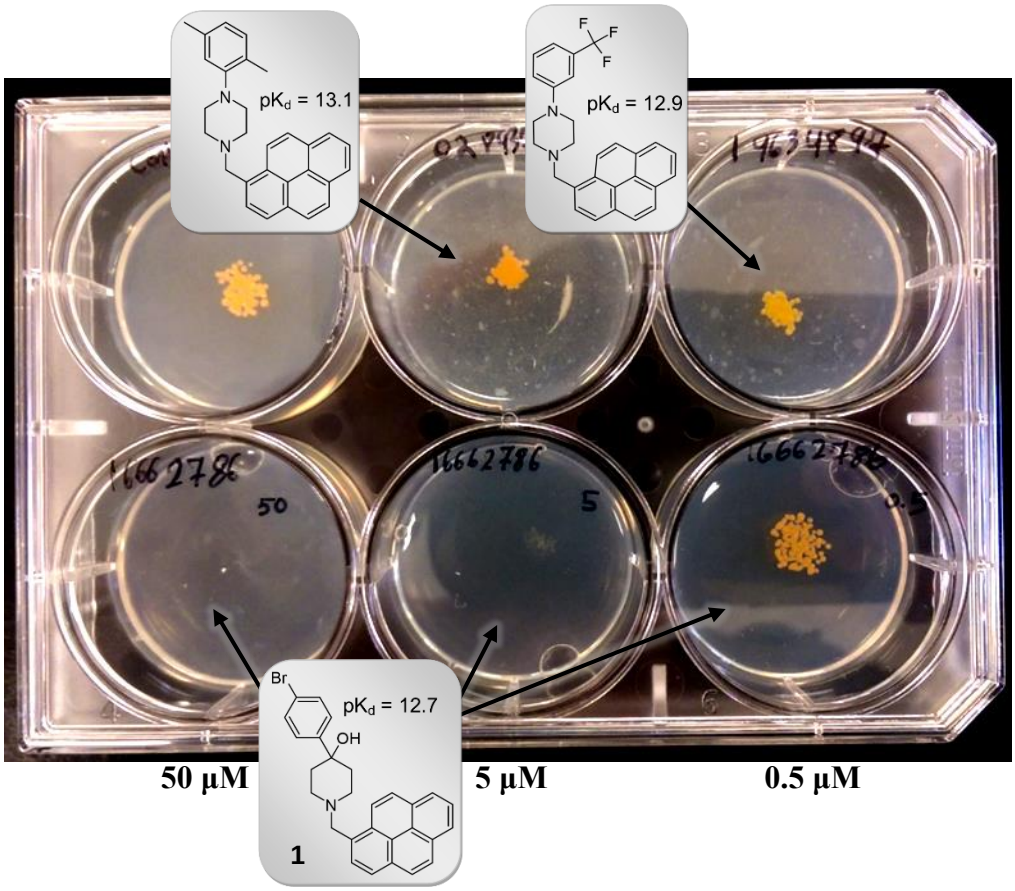

Figure 4: The results of an in vitro test of the effect of three inhibitors on M. bovis growth. These inhibitors were predicted to have high pK$_d$ by virtual screen. The bottom left two wells, treated with compound **1** in concentrations of 50 and 5 µM, showed no bacterial growth.

Compound **1** is shown, along with the docking results proposed in the screen, in Figure 5. The docking results show the predicted way the inhibitor should bind to the enzyme. Compound **1** is displayed in gray, and the native substrate for the enzyme, acyl chains, are shown in blue and red. The bromoaryl ring of the inhibitor occupies the hydrophobic channel that would otherwise contain the alkyl chain of the acyl substrate, preventing its binding. The aromatic pyrenyl group fits in a pocket adjacent to the active site residues.

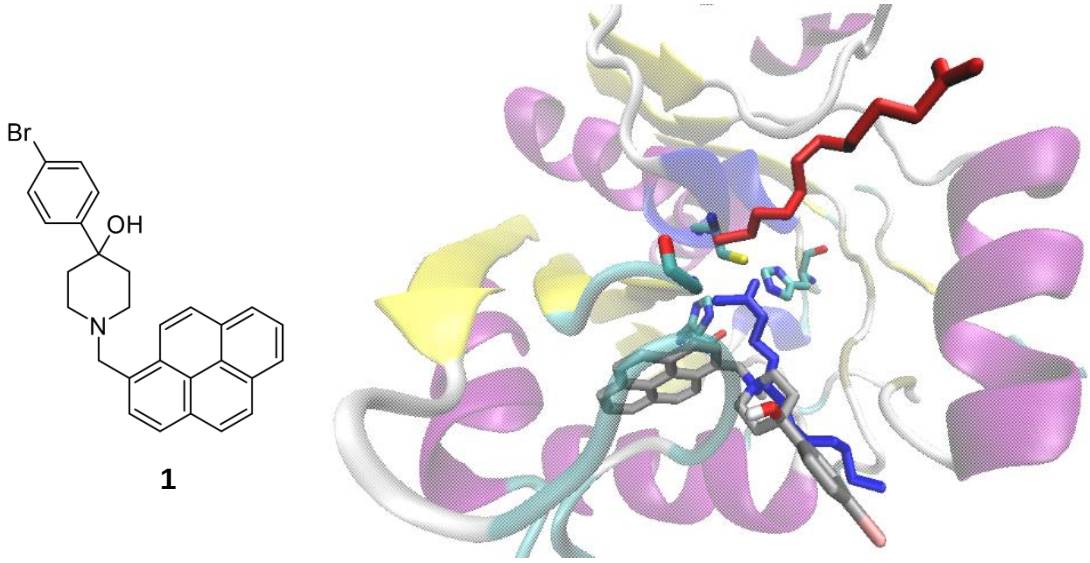

Figure 5: The molecular structure of **1**, a suspected inhibitor of KasA, along with its proposed docking configuration. Compound **1** is shown docked in gray, with the typical binding of the acyl chain substrate shown superimposed in blue and red. The bromoaryl ring occupies the same hydrophobic channel as the acyl chain substrate, preventing binding.

The purpose of this work is to create a library of derivatives of the lead compound with varying substituents to be used in a structure-activity relationship study. Similar compounds to **1** may have greater affinity for the enzyme, may bind more easily, or may have different effects on other biological processes. They may also have no effect on the enzyme, as seen in the failed inhibitors in Figure 4, whose structures were similar to compound **1**. To test the importance of each part of the structure, modifications can be made to the structure at position 1 and position 4 on the central piperidine ring. Positions which can be modified and the various alternative groups for each position are shown in Figure 6.

By varying these substituents, the effect of each position on the inhibitor's binding to KasA can be studied. The bromoaryl group at position 4 can be changed for a chlorophenyl, trifluoromethylphenyl, or phenyl group. These changes would test the

significance of the bromine extending from the hydrophobic channel. The hydroxy group at position 4 can be exchanged for a hydrogen to observe if hydrogen bonding is significant to the inhibitor's success. Finally, the large pyrene group at position 1 can be changed for smaller aryl groups like naphthylmethyl and benzyl, which may have different solubility properties and are less expensive to manufacture. Additionally, varying these groups to find different structures with similar inhibitory ability may provide viable alternatives with less toxicity to humans or other unwanted effects.

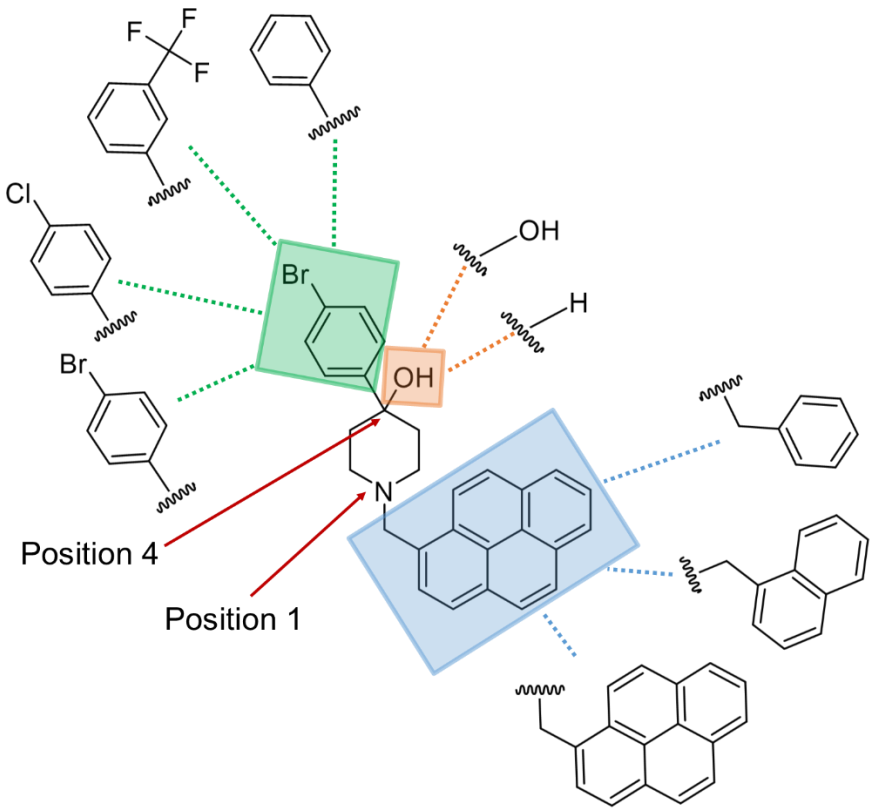

Figure 6: Compound **1**, is shown with each region targeted for modification hilighted. The bromophenyl group at position 4 shown highlighted in green with its replacement structures, chlorophenyl, trifluoromethylphenyl, and phenyl. The pyrenemethyl group is in blue at the 1 position of the piperdine backbone, with its replacements of phenylmethyl and naphthylmethyl. Finally, the hydroxy group targeted at position 4 is in orange, and is targeted for replacement with hydrogen.

To investigate the significance of the structural components of compound **1**, a collection of similar compounds will be synthesized with variations in position 1 and 4 on the piperidine backbone. In this work, two general approaches were used for the modification of the lead compound, outlined in Scheme 1. The alkylation-first approach follows the top line of the scheme. The 1 position of **2** is modified by alkylation to form **4a-c**, installing the desired aryl group. Next, a Grignard or alkyllithium reagent installs the aryl halide at position 4 of **4a-c**.

The second line of the synthesis uses an alkylation-second approach. It reverses the order of modifications on the piperidine ring, modifying position 4 first, followed by position 1. In this approach **7** is converted to **8a-d** is with a Grignard or alkyllithium reagent. The protecting group is removed with acid to form **9**, and an alkylation is performed to install the aryl group to generate **1, 6a-k**.

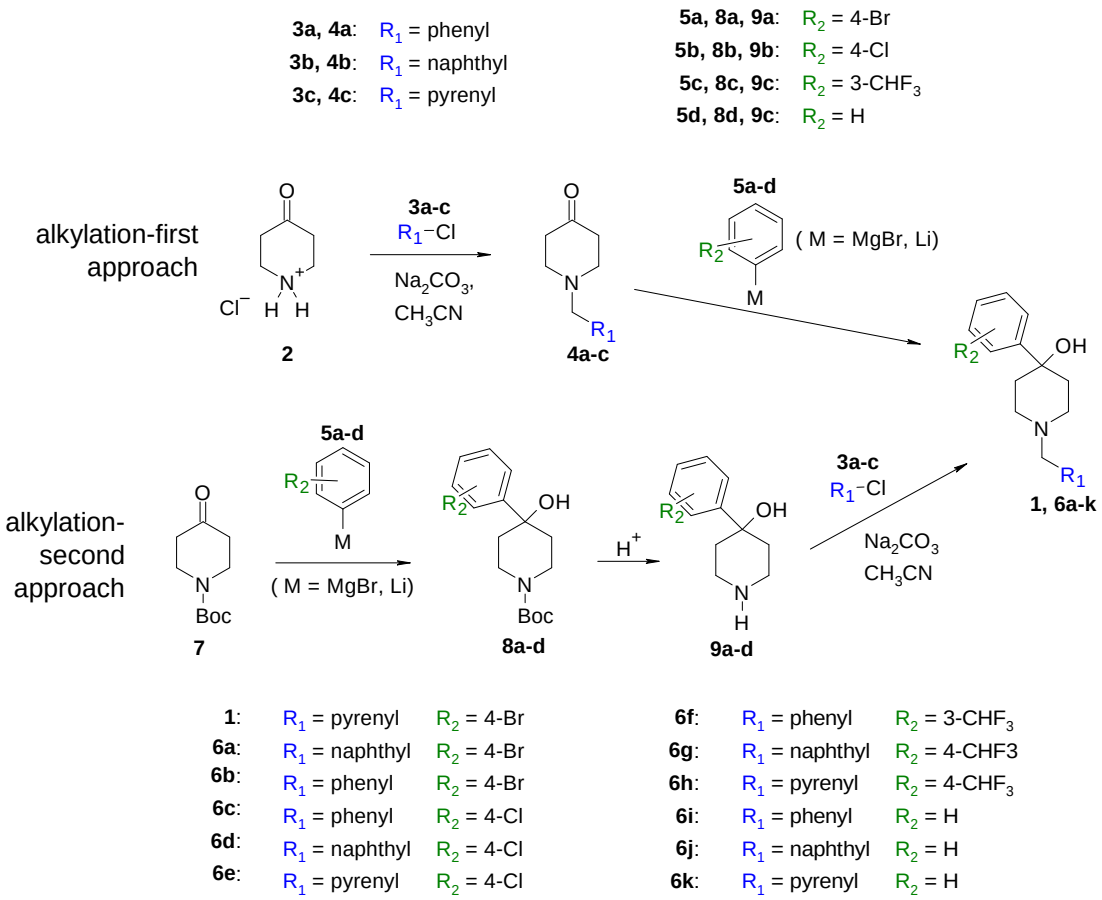

1:	R_1 = pyrenyl	R_2 = 4-Br
6a:	R_1 = naphthyl	R_2 = 4-Br
6b:	R_1 = phenyl	R_2 = 4-Br
6c:	R_1 = phenyl	R_2 = 4-Cl
6d:	R_1 = naphthyl	R_2 = 4-Cl
6e:	R_1 = pyrenyl	R_2 = 4-Cl
6f:	R_1 = phenyl	R_2 = 3-CHF_3
6g:	R_1 = naphthyl	R_2 = 4-CHF3
6h:	R_1 = pyrenyl	R_2 = 4-CHF_3
6i:	R_1 = phenyl	R_2 = H
6j:	R_1 = naphthyl	R_2 = H
6k:	R_1 = pyrenyl	R_2 = H

Scheme 1: Two possible approaches to synthesis of derivatives of compound **1** with modifications at the 1 and 4 positions.

II. Results and Discussion

Grignard and Lithiation Reactions with Piperidones

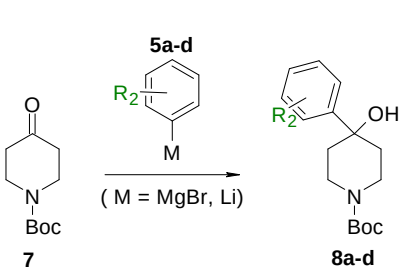

5a, 8a: R_2 = 4-Br
5b, 8b: R_2 = 4-Cl
5c, 8c: R_2 = 3-CHF_3
5d, 8d: R_2 = H

3a, 4a: R_1 = phenyl
3b, 4b: R_1 = naphthyl
3c, 4c: R_1 = pyrenyl

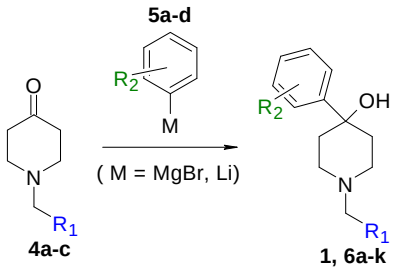

1:	R_1 = pyrenyl	R_2 = 4-Br
6a:	R_1 = naphthyl	R_2 = 4-Br
6b:	R_1 = phenyl	R_2 = 4-Br
6c:	R_1 = phenyl	R_2 = 4-Cl
6d:	R_1 = naphthyl	R_2 = 4-Cl
6e:	R_1 = pyrenyl	R_2 = 4-Cl
6f:	R_1 = phenyl	R_2 = 3-CHF_3
6g:	R_1 = naphthyl	R_2 = 4-CHF3
6h:	R_1 = pyrenyl	R_2 = 4-CHF_3
6i:	R_1 = phenyl	R_2 = H
6j:	R_1 = naphthyl	R_2 = H
6k:	R_1 = pyrenyl	R_2 = H

Scheme 2: The two approaches to modification of the aryl group at the 4 position of the piperidine backbone.

Both approaches outlined in Scheme 1 required a modification at the 4-position of the piperidine backbone, using either a Grignard reagent or an alkyllithium to add the desired R_2 group at the carbonyl. These syntheses are shown in Scheme 2. The major difference between the two approaches is the presence of either the aryl group of the final intended product already installed in position 1, or a *tert*-butyloxycarbonyl (Boc) protecting group in this position to be removed later. These reactions were largely unsuccessful, and reaction monitoring by gas chromatography/mass spectrometry (GCMS) was used to attempt to discover why these reactions did not work as expected.

Grignard Reaction

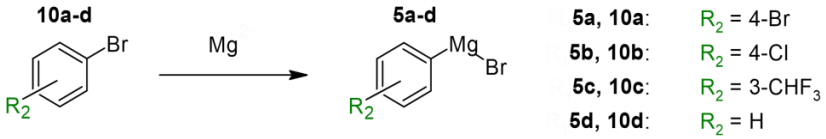

Scheme 3: Planned synthesis of the Grignard reagents.

The Grignard approach was attempted for the creation of **6b** from **4a**. The first step of this reaction, the generation of the Grignard reagent **5a** from **10a** is outlined in Scheme 3. The reaction was carried out under dry conditions, and during reflux of **5a** with magnesium, the magnesium did appear to be consumed. However, upon reaction a mixture of products was generated and large amounts of **5a** were present. To test the formation of the Grignard reagent, the first step of the reaction (Scheme 3) was repeated and monitored by GCMS over 30-minute intervals during reflux.

Samples of the reaction were quenched in water. Successful formation of the Grignard reagent could be monitored by the presence of the quenched product, bromobenzene. The chromatograms of the reaction of **10a** showed large amounts of unreacted **10a** during the initial 1.5 hours of reaction time, and after 24 hours of stirring little change was observed in the composition of the mixture.

This monitoring process was repeated again with the addition of iodine as a catalyst for the reaction, but the result was the same, with **10a** remaining largely unreacted. GC chromatograms (Figure 7) showed the relative growth of the bromobenzene signal after workup to a signal of equal strength to the starting material. Without knowing the relative response factor between the two substances, it is not

possible to draw significant conclusions about the extent to which this reaction went to completion, however greater conversion is desired.

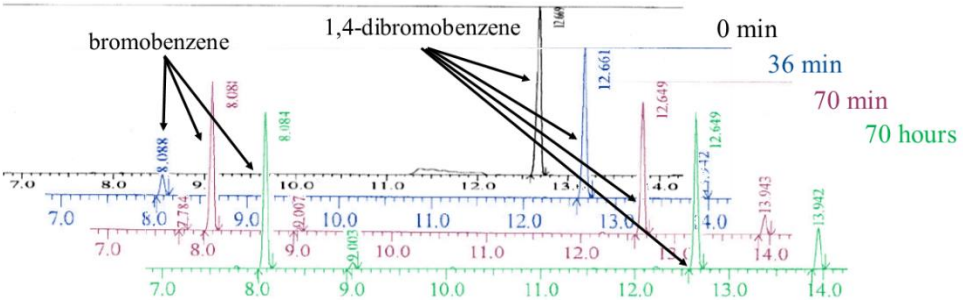

Figure 7: Four chromatograms from the reaction monitoring of the Grignard reaction of **10a** (1,4 dibromobenzene). The bromobenzene peak, indicating formation of product, has an equal peak area to the **10a** peak at 70 minutes, and no improvement is seen after 70 hours.

Using **10d**, a monosubstituted bromobenzene, as a starting material to create a Grignard reagent to used for the conversion of **7** to **8d** was met with more success. A GC chromatogram of the crude product of this reaction appeared relatively pure, with only one significant peak. The mass spectrum also supported the formation of the intended product. The M^+ of the species in the chromatogram was 277, which is the expected mass of the intended product of this reaction. The spectrum and chromatogram are shown in Figure 8.

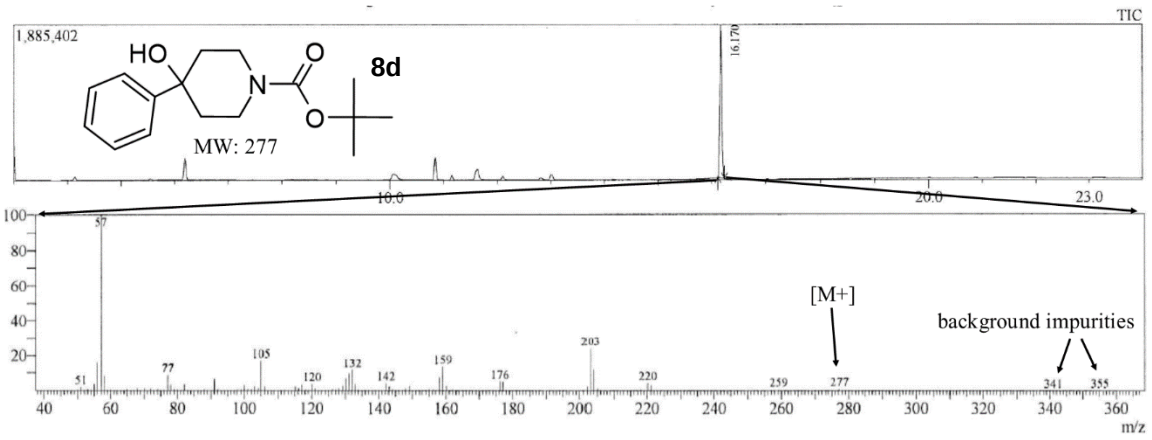

Figure 8: The chromatogram and mass spectrum of the product of a phenyl Grignard made from a mono-brominated benzene starting material with boc-piperidone. The mass of the molecular ion of the species in the mass spectrum is the same as the mass of the expected product.

Overall, these results suggest that **10a** may be a challenge for conversion into a Grignard reagent. This is an interesting result, as the literature suggests that 1,4-dibromobenzene should react comparably to the monosubstituted aryl halide in tetrahydrofuran (THF) solvent.[16] Possible development of this Grignard reaction could include testing a different dihalogenated starting material, like a bromoiodobenzene, in order to compare the performance of the reactions under similar conditions. Alternatively, a different exchange reagent from magnesium metal may have better results.[17] This would allow greater insight into the effect of bromine disubstitution on this reaction. Also, quantitative monitoring of the reaction by GCMS would aid in understanding the success of the reaction.

Lithiation Reaction

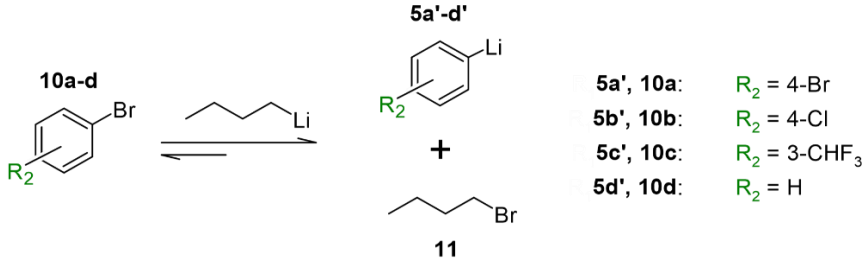

Scheme 4: The lithium-halogen exchange using n-butyllithium.

The second approach to modification at the 4 position of the piperidine ring was to create a desired organolithium reagent to add an aryl group at the carbonyl by using a lithium-halogen exchange reaction. The first step of this process is outlined in Scheme 4. In this reaction, the carbanion of the n-BuLi reagent forms an ionic intermediate by attacking the halogen of **10a-d**.[18] This intermediate can then generate **5a'-d'** and **11**. Although not used in further synthesis, **11** was used as a marker for successful lithium-halogen exchange.

Initial trials of this reaction followed Scheme 2, using **5a'** to add an aryl halide to **4a**. In one flask, the n-BuLi was added to **10a** in -78°C tetrahydrofuran. The low temperature reduces the possibility of unwanted reactions with the solvent.[19] After the dropwise addition of the n-BuLi, **4a** was added. Workup of the reaction after adding **4a** showed a mixture of products and remaining starting material in TLC. Because of this, the first step of the reaction, shown in Scheme 4, was repeated and monitored by GCMS to try to optimize the reaction. When initial trials showed large amounts of the unreacted **10a** starting material and no **11** present, the butyllithium was titrated with diphenylacetic acid to determine its concentration. As could be expected due to its high reactivity, the actual concentration of nBuLi reagent had decreased to half the original concentration.

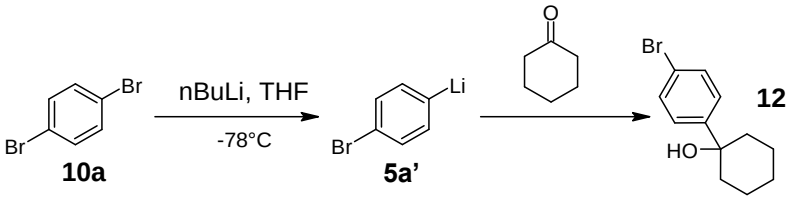

Scheme 5: A model reaction was attempted using cyclohexanone instead of the more expensive piperidone.

In further testing, a model reaction was used with a cheaper alternative to **4a**, cyclohexanone, as shown in Scheme 5. The reaction used an adjusted volume of nBuLi, and after the lithium-halogen exchange step, cyclohexanone (1 equiv) was added to the reaction mixture. Monitoring of the lithium halogen exchange reaction showed some **11** formed, and no detectable **10a**. After addition of cyclohexanone the reaction was worked up and characterized with GCMS. The labeled chromatogram in Figure 9 shows that **12** was not formed, and many of the products were from unintended side reactions.

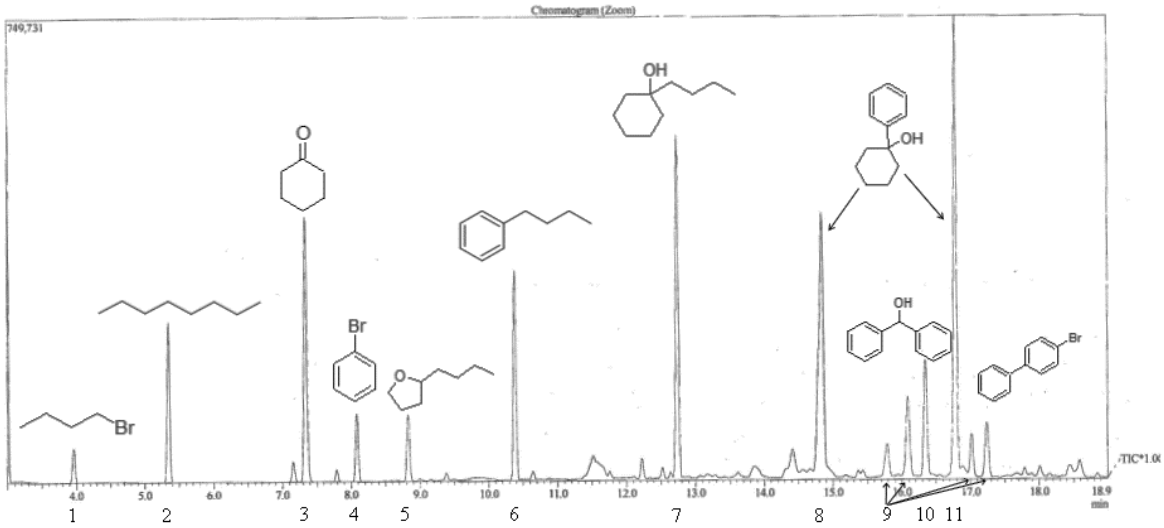

Figure 9: A chromatogram of the reaction of **10a** with n-BuLi, followed by cyclohexanone. Selected peaks are labeled to demonstrate the unwanted side reactions that occurred.

Although there was no unreacted **10a** in the chromatogram, very little bromobutane, the marker for successful lithium-halogen exchange, was found. Side reactions with the n-BuLi itself are seen in peaks 2, 5, 6, and 7, including reactions with the solvent. **5a'** reacting with itself is seen in peaks 9 and 10. A large peak of unreacted cyclohexanone is in peak 3, and finally a compound similar to **12**, but lacking bromine, is seen formed in peaks 8 and 11. Although quantitative information about the relative

concentrations of these side products, unreacted starting material, and desired products cannot be determined from the chromatogram, the overall selectivity of this reaction is certainly seen to be poor.

The reaction was further tested with various mixtures of product and unreacted starting material and substitution of **10a** with 1-bromo-4-iodobenzene. The reactions all showed large quantities of the nBuLi reacting with itself or forming structures like butylbenzene. This reaction is an interesting route to creating derivatives of the target compound, and substitution at the 4 position of the piperidine backbone is very desirable. This reaction could increase the variety of substituents that can be installed and reduce costs by allowing the desired structures to be generated from simpler starting materials. Future development of the lithium-halogen exchange could involve controlling the rate of addition of the n-BuLi to the aryl halide starting material and controlling the time of addition of the ketone. The role of the concentration of the reactants could also be investigated.

Amine Alkylations of 4-Piperidinols

The second part of the strategy for modification of the lead compound involved modification at the 1 position of the piperidine backbone. The method used in both the alkylation-first and alkylation-second approach is an amine alkylation, an S_N2 type reaction where the amine of the piperidinol acts as a nucleophile with an alkyl halide. The reaction, specifically from the alkylation-second approach, is outlined in Scheme 6.

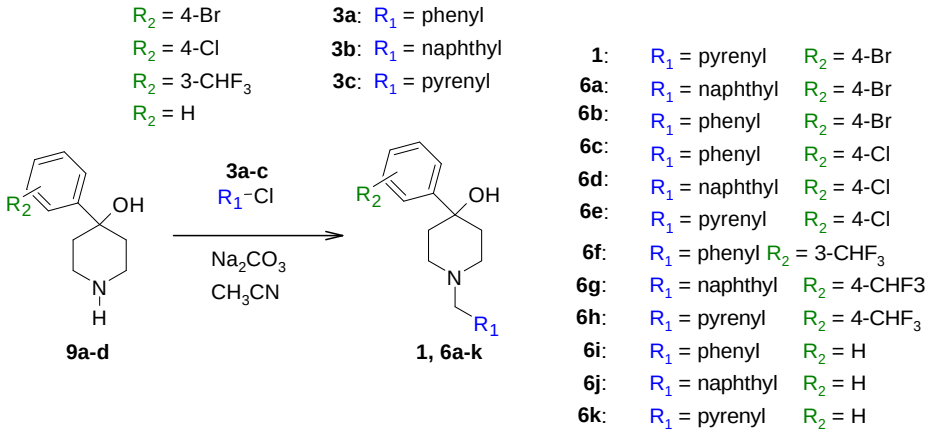

Scheme 6: The amine alkylation reaction.

To save time and cost, this reaction used commercially available **9a-d** starting material and aryl halides **3a-c** to create 12 derivatives, **1, 6a-k**. The reactants were refluxed with sodium carbonate in acetonitrile for at least one hour before gravity filtration and evaporation of the solvent. GCMS monitoring of the reaction showed the reaction generally completed within two hours. The reaction appeared to not have significant side reactions. Chromatograms of successful reactions showed only starting material and the desired product. Additionally, the reaction did not appear to generate the quaternary amine product, shown in Figure 10.

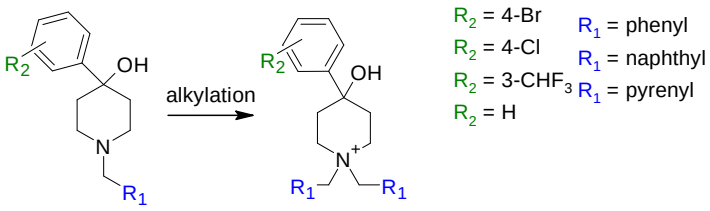

Figure 10: During amine alkylation, a quaternary ammonium cation can be formed. This unwanted product was not observed.

A likely reason that this reaction did not proceed to the quaternary ammonium cation is the steric bulk of the aryl halide R_2 groups. Despite being similarly basic to its secondary amine counterpart, the tertiary amine does not participate in a second S_N2 reaction with the aryl chloride substrate, which is well supported by the literature in which alkylation of a piperidine to a tertiary benzylic amine is often shown with high yields under similar reaction conditions.[20,21]

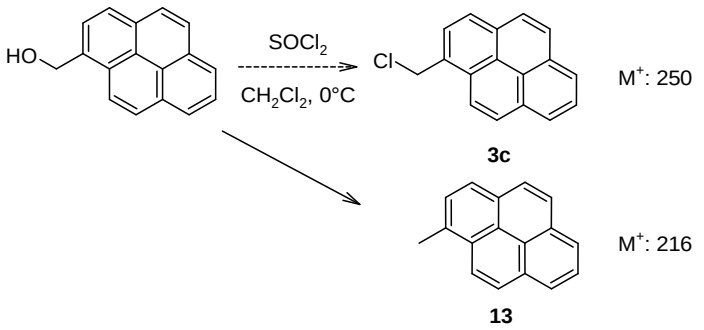

Figure 11: The synthesis of **3c** and the unintended product **13**.

Unfortunately, the pyrenyl derivatives **1**, **6e**, **6h** and **6k** were not successfully synthesized. GCMS of **3c** showed that the reaction used to generate this starting material

may have generated **13** instead of the aryl chloride, as shown in Figure 11. The mass spectra of the pyrene starting material is shown in Figure 12. The molecular ion mass (M^+) is 216, which is identical to the molecular mass of 1-methylpyrene. The expected (1-chloromethyl)pyrene should have had a M^+ of 250. Before this starting reagent had been characterized by GCMS, various pyrene alkylations were attempted, but none successfully generated the desired product.

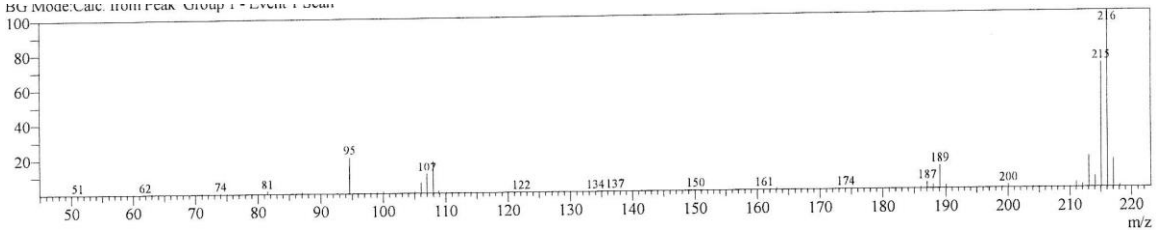

Figure 12: Mass spectrum of **13**. This product was the result of an unsuccessful attempt to synthesize **3c**.

The products were all purified by column chromatography, typically in hexanes/ethyl acetate. TLC of most compounds on silica gave good relative migration (R_f) separation between the product and the nearest impurities, though streaking of the amine was common. Identifying the chromatography fractions by TLC was made more difficult by the resolution of identical compounds (as determined by GCMS) at different R_f. This may have been due to the presence of stereoisomers of the compound, however pyramidal inversion of nitrogen should prevent the resolution of these isomers, as the R/S configuration of amines rapidly interconverts at room temperature by a quantum tunneling mechanism. However, intramolecular hydrogen bonding has been shown to slow this interconversion significantly.[22] A boat conformation of the piperidine backbone could create such a favorable interaction between the lone pair electrons of the amine and

the hydrogen of the hydroxy group, shown in Figure 13. This would generate a less flat structure than the chair conformation where both bulky aryl groups are equatorial. This curved structure would have a higher R_f due to fewer van der Waals interactions between the structure and the TLC substrate. Though this would be an interesting property to investigate further, the significance of this to synthesis is largely that higher yields were possible by using GCMS to identify fractions instead of TLC.

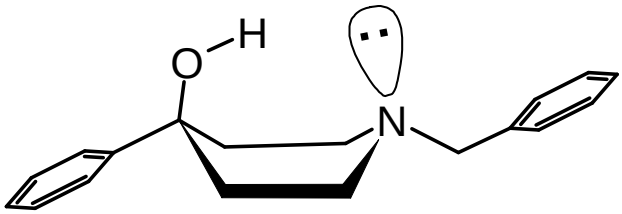

Figure 13: A boat conformation of **6i**. The interaction between the lone pair of the amine and the hydrogen of the hydroxy group may result in intramolecular hydrogen bonding and a slower inversion of the amine.

The yields of the amine alkylation reaction are summarized in Figure 14. Generally, the smaller aryl halide electrophiles had higher yields than their bulkier counterparts, with one exception of 4-(4-chloro)phenyl-1-naphthylmethyl-4-piperidinol **(6)**. Overall this reaction is effective in derivatizing the lead compound in the 1 position. Future derivatives can be created based on this alkylation reaction.

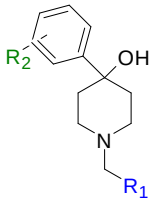

R_2 = 4-Br
R_2 = 4-Cl
R_2 = 3-CHF_3
R_2 = H

R_1 = benzyl
R_1 = naphthyl
R_1 = pyrenyl

R^2	R^1 benzyl	naphthyl	pyrenyl
H	57	52	-
4-Br	64	58	-
4-Cl	63	85	-
3-CHF_3	77	TBD	-

Figure 14: The percent yields of each alkylation reaction after purification by flash chromatography.

Organosilane Reduction of Hydroxy Group

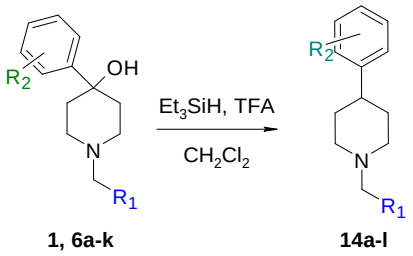

1, 6a-k **14a-l**

1:	R_1 = pyrenyl	R_2 = 4-Br
6a:	R_1 = naphthyl	R_2 = 4-Br
6b:	R_1 = phenyl	R_2 = 4-Br
6c:	R_1 = phenyl	R_2 = 4-Cl
6d:	R_1 = naphthyl	R_2 = 4-Cl
6e:	R_1 = pyrenyl	R_2 = 4-Cl
6f:	R_1 = phenyl	R_2 = 3-CHF_3
6g:	R_1 = naphthyl	R_2 = 4-CHF3
6h:	R_1 = pyrenyl	R_2 = 4-CHF_3
6i:	R_1 = phenyl	R_2 = H
6j:	R_1 = naphthyl	R_2 = H
6k:	R_1 = pyrenyl	R_2 = H

Scheme 6: The overall reaction for the triethylsilane reduction of the hydroxy group.

Following the creation of **1, 6a-k**, reduction of the hydoxy group at position 4 was also attempted to generate **14a-l**. The approach (Scheme 6) used silane reduction.[23] Triethylsilane in trifluoroacetic acid was used to remove the hydroxy group. One equivalent of **1, 6a-k** was added to triethyl silane (9.5 equivalents) and trifluoroacetic acid (6.5 equivalents) and stirred overnight. Workup of the mixture was performed with sodium hydroxide, followed by purification via column chromatography. Initially, the reduction of **6** appeared to have been successful. Product formation was checked both by TLC and GCMS. In TLC, a higher R_f spot was generated relative to the starting material, which is expected for the less polar product on silica backed plates. However, mass spectrometry of the starting material and the product showed M^+ of 199 and 217. The mass spectra of the two largest peaks on the mass chromatogram of the first attempt at reducing **6i** are shown in Figure 15.

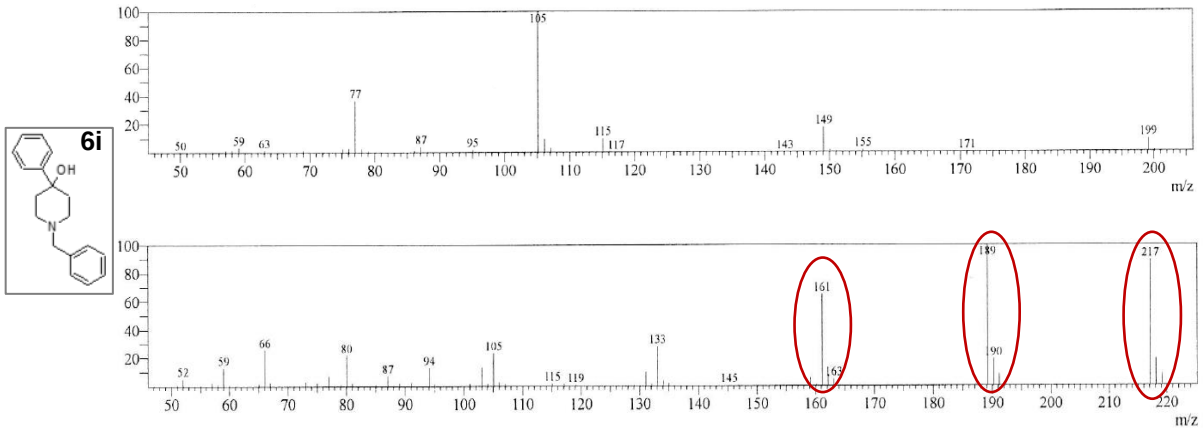

Figure 15: The mass spectra of two unexpected products of the silane reduction of **8**. The circled peaks and their M+1 and M+2 peaks suggest that a silicon atom may be present in the molecule. Additional structural information may be possible with NMR analysis.

One of the products of the first reaction of **6i** appeared to include silicon (indicated by the presence of M-28 peaks and the relatively large M+1 and M+2 peaks) which would have come from the triethylsilane. Silane reduction of alcohols is thought to proceed by the mechanism shown in Figure 16.[24,25] The reaction requires dry conditions to avoid the formation of silanols.

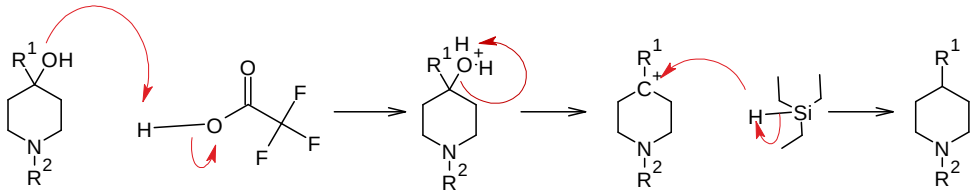

Figure 16: One proposed mechanism for the silane reduction, which proceeds through a carbocation intermediate.

A second attempt at this reduction, this time using **6j,** appeared to have a 12% yield. The mass spectrum of this product is shown in Figure 17. The M^+ of the product is two amu less than expected. The reaction mixture had dried during stirring, so addition of a small amount of dichloromethane solvent was used in the proceeding reactions in an attempt to improve the yield.

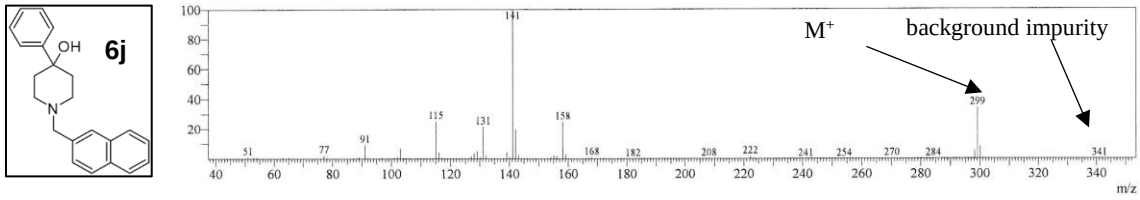

Figure 17: A mass spectrum of the product of the reduction of **6j**. The M^+ peak at 299 is two less than the expected mass, 301.

The first attempted reaction using dichloromethane solvent with **6i** was unsuccessful, with only traces of possible product. This can potentially be attributed to the use of wet dichloromethane. The reaction was repeated with dry dichloromethane, and although it was not purified to find the yield, GCMS of the products suggest that the desired product may have been formed. A comparison of the two largest peaks in the chromatogram for the reaction of **6i** in dry dichloromethane is shown in Figure 18. The two molecular ions are 249 and 267, with the lower M^+ corresponding to the reduced compound. GCMS of the starting material, **6i**, also has an M^+ of 267, with an identical fragmentation pattern to the other abundant peak in the chromatogram of the reduction product mixture, demonstrating that unreacted starting material remained.

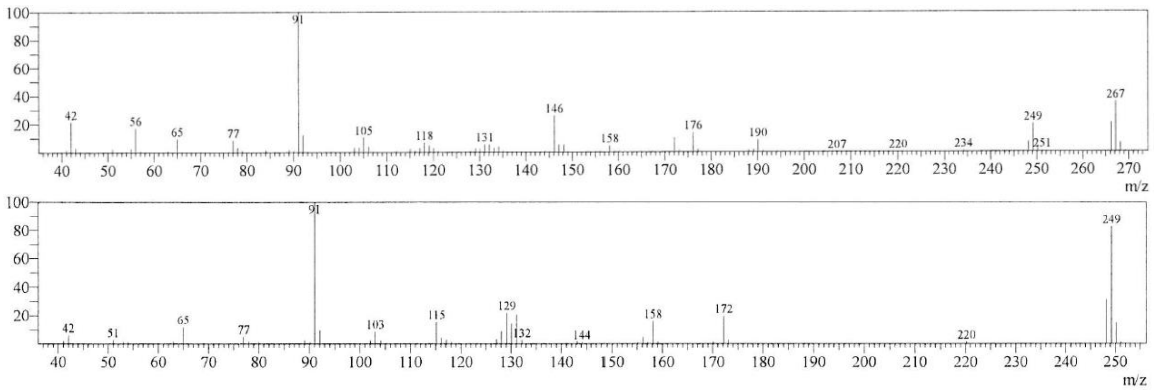

Figure 18: The mass spectra of the two products of the reaction of **6i** in dry acetonitrile. The fragmentation pattern shown in the top spectrum is identical to that of the starting material. The difference of 18 between the two spectra could be attributed to the loss of the hydroxy group.

Interestingly, the product of the reduction of both **6i** and **6j** resulted in products whose m/z was smaller than expected by two AMU. This lower molecular ion mass may indicate that an elimination reaction is occurring, which is creating an alkene between the 3 and 4 carbons of the piperidine ring, as shown in Figure 19. This alkene would create a flat region on the molecule that may greatly reduce the effectiveness of this structure as an inhibitor of KasA.

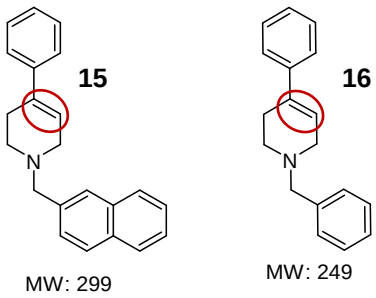

Figure 18: The possible products of the reduction of **7** and **6**, respectively. The potential unintended alkene locations are shown circled in red. The molecular masses of these two compounds corresponds better to the mass spectra than the alkane products.

Overall this reaction requires additional optimization. Dry solvent and glassware are critical. Low yields compared to literature (67% reported with a similar structure)

may be due to properties of the starting piperidinol, but the triethylsilane used may also have degraded.[23] Investigation into the structures formed in Figure 15 may give insight into how to further improve the reaction conditions and avoid unwanted side reactions. Importantly, the reaction must be controlled to avoid the elimination product so that the typical geometry of the piperidine ring can remain.

III. Future Work

For future work, in order to create a diverse collection of compounds for testing, several approaches are proposed, each with the aim of modifying either the 1 or 4 position of the central piperidine ring in the lead compound. There are three new approaches for modification of the 1 position. First, a Grignard reaction will be attempted, using different functionalized iodo-aryl compounds and isopropyl magnesium chloride, as in Scheme 4. This scheme has been shown to be more effective at creating aryl Grignard reagents than a traditional Grignard reaction.[17]

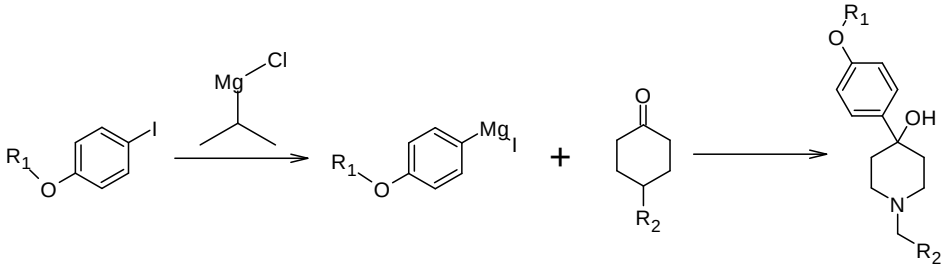

Scheme 7: Grignard with isopropyl magnesium chloride.

The starting aryl chloride can be purchased or created by starting with 4-iodophenol and performing a Williamson ether reaction to replace the hydroxide group with different alkoxy groups, as shown in Scheme 5.[26,27] Adding alkyl chains to the compound may aid in enzyme inhibition because they mimic the fatty acid chains present in mycolic acid synthesis.[12]

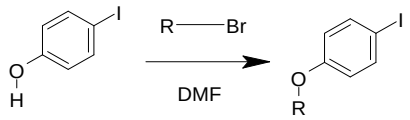

Scheme 8: Williamson ether reaction.

The second approach to modifying the 4-position is a copper-catalyzed azide-alkyne cycloaddition (CuAAC), or "click" reaction, which would replace the benzyl chloride of compound one with a functionalized triazole, as in Scheme 6.

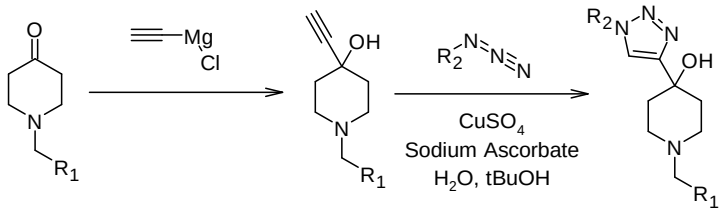

Scheme 9: Cu(I)-catalyzed azide-alkyne cycloaddition.

Importantly, 1-chloromethylpyrene must be synthesized to create critical pyrenyl derivatives via amine alkylation. The 1-chloromethylpyrene synthesis used is shown in scheme 10.[28] This reaction was unsuccessful in previous work, but this reaction should be robust. Additional attempts should result in synthesis of the desired compound.

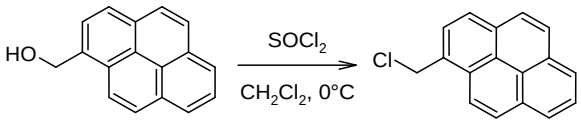

Scheme 10: The synthesis of (1-chloromethyl)pyrene.

In the long-term, the library of derivatives of the lead compound will be tested for affinity to KasA, and their effects on nonpathogenic mycobacteria will be observed. These compounds may aid in the continuing search for potent inhibitors that can aid in halting MDR-TB.

IV. Experimental

Suppliers and purities of all chemicals are listed in Appendix I. All reagents were used as received unless noted. Column chromatography was conducted on a Biotage Isolera One flash system. Gas Chromatography Mass Spectrometry was performed with a Shimadzu GCMS-QP5050A Gas Chromatograph/Mass Spectrometer. Anhydrous tetrahydrofuran (THF) and dichloromethane were dispensed from an MBraun Solvent Purification System.

1-Benzyl-4-(4-bromophenyl)-4-piperidinol (6b). In a 50 mL round bottomed flask with magnetic stir bar and condenser, 268 mg (1.04 mmol, 1.01 eq) of 4-(4-bromophenyl)-4-piperidinol, 131 mg (1.03 mmol, 1.00 eq) of benzyl chloride, and 326 mg (3.07 mmol, 2.98 eq) sodium carbonate were added. Acetontrile (10 mL) was added as solvent. The mixture was refluxed for 16 hours, and the crude mixture was monitored by TLC (50% hexanes in ethyl acetate, product R_f = 0.29), showing product formation. The reaction mixture was gravity filtered and the solids were washed with an additional 20 mL of acetonitrile. The solvent was then removed under vacuum. The product was purified by flash chromatography (SNAP Ultra 10g column, dichloromethane/methanol gradient). Crude yield: 95%; purified yield: 62%. MS *m/z*: [M^+] calcd 346; found 346

1-Benzyl-4-(4-chlorophenyl) -4-piperidinol (6c). In a 50 mL round bottomed flask with a magnetic stir bar and condenser, 317 mg (2.99 mmol, 2.93 eq) sodium carbonate, 225 mg (1.06 mmol, 1.03 eq) 4-(4-chlorophenyl)-4-piperidinol, and 137 mg (1.02 mmol, 1.00 eq) of benzyl chloride was refluxed in 10 mL of acetonitrile for 16 hours. The reaction mixture was monitored by TLC (9% methanol in dichloromethane, product R_f = 0.30) and gravity filtered. The waste solids were washed with 20 mL of acetonitrile, and

solvent removed under vacuum. The crude product was purified by flash chromatography (SNAP Ultra 10g column, dichloromethane/methanol gradient). Crude yield: 99%, purified yield: 63%. MS *m/z*: [M^+] calcd 301; found 301

4-(4-Chlorophenyl)-1-(1-naphthylmethyl)-4-piperidinol (6d). In a 50 mL round bottomed flask with stir bar and condenser, 319 mg (3.01 mmol, 3.01 eq) sodium carbonate, 224 mg (1.06 mmol, 1.06 eq) 4-(4-chlorophenyl)-4-piperidinol, and 177 mg (1.00 mmol, 1.00 eq) 1-(chloromethyl)naphthalene were refluxed in 10 mL of acetonitrile for 19 hours, at which time the reaction mixture was monitored by TLC (9% methanol in dichloromethane, product R_f = 0.48) and gravity filtered. The waste solids were washed with 20 mL of acetonitrile and the solvent removed under vacuum. The product was purified by flash chromatography (SNAP Ultra 10g column, dichloromethane/methanol gradient). Crude yield: 99%, purified yield: 85%. MS *m/z*: [M^+] calcd 351; found 351

1-Benzyl 4-[3-(trifluoromethyl)phenyl]-4-piperidinol (6f). In a 100 mL round bottomed flask with magnetic stir bar and condenser, 270 mg (2.13 mmol, 1.01 eq) benzyl chloride, 517 mg (2.11 mmol, 1.00 eq) 4-[3-(trifluoromethyl)phenyl]-4-piperidinol, and 639 mg (6.02 mmol, 2.85 eq) sodium carbonate were refluxed in 20 mL acetonitrile for 24 hours. The reaction was monitored by GCMS (m/z 335) showing product formation during the first hour of the reaction. TLC confirmed product formation (50% hexanes in ethyl acetate, product R_f = 0.31). The mixture was gravity filtered and the solid waste was washed with 20 mL acetonitrile. The solvent was removed under vacuum. Automated flash chromatography (10 g SNAP Ultra, hexanes/ethyl acetate gradient) was used for purification. Crude yield: 88%, purified yield: 73%. MS *m/z*: [M^+] calcd 335.36; found 335.10

1-Benzyl-4-phenyl-4-piperidinol (6i). In a 50 mL round bottomed flask with magnetic stir bar and condenser, 341 mg (3.22 mmol, 2.98 eq) sodium carbonate, 192 mg (1.08 mmol, 1.00 eq) 4-hydroxy-4-phenylpiperidine, and 131 mg (1.03 mmol, 0.95 eq) benzyl chloride were refluxed in 10 mL acetonitrile for 20 hours and then monitored by TLC (50% hexanes in ethyl acetate, product R_f = 0.25). The mixture was gravity filtered and the waste solids were washed with 20 mL acetonitrile. The solvent was removed under vacuum, and the product was purified by automated flash chromatography (10 g SNAP Ultra column, hexanes/ethyl acetate gradient). Crude yield: 94%, purified yield: 57%. MS *m/z*: [M^+] calcd 267; found 267

1-(1-Naphthylmethyl)-4-phenyl-4-piperidinol (6j). In a 100 mL round bottomed flask with stir bar and condenser, 372 mg (2.11 mmol, 1.00 eq) 1-(chloromethyl)naphthalene, 381 mg (2.15 mmol, 1.02 eq) 4-hydroxy-4-phenylpiperidine, and 641 mg (6.04 mmol, 2.86 eq) sodium carbonate was refluxed in 20 mL acetonitrile for 18 hours. The reaction was then monitored by TLC (50% hexanes in ethyl acetate, product R_f = 0.48) and gravity filtered. The waste solids were washed with 20 mL acetonitrile and the solvent was removed under vacuum. Automated flash chromatography (10 g SNAP Ultra column, hexane/ethyl acetate gradient) was used to purify the product. Crude yield: 99%, purified yield: 52%. MS *m/z*: [M^+] calcd 317.42; found 317.25

1-Boc-4-phenyl-4-piperidinol (8d). In a dry round bottomed flask with Claisen adapter, condensing tube and addition funnel, 245 mg (10.1 mmol,1.00 eq) magnesium turnings were placed in 3 mL dry THF. The vessel was heated to 70 °C. Dropwise through the addition funnel, 1.63 g bromobenzene (10.4 mmol, 1.03 eq), was added in 4 mL of additional dry THF. After 30 minutes of stirring, the reaction was cooled and 2.003 g

(10.1 mmol, 1.00 eq) boc-piperidone dissolved in 3 mL THF was added through the addition funnel dropwise. The reaction was heated again for 15 minutes, then cooled. The product mixture was quenched with 8 mL H_2O and 1 mL of 1M ammonium chloride. It was then extracted with 3x20 mL ethyl acetate and dried over magnesium sulfate. The crude product was gravity filtered and characterized by GCMS. Crude yield: 75% MS *m/z*: [M^+] calcd 277; found 277

1-Methylpyrene (13). In a 250 mL round bottomed flask with magnetic stir bar and a drying tube, 2.13 g (9.18 mmol, 1.00 eq) of 1-pyrenemethanol and 1.6 mL (22 mmol, 2.4 eq) of thionyl chloride was dissolved in 50.5 mL of dichloromethane and stirred at room temperature. A TLC after one hour showed a partial reaction (80% hexane in ethyl acetate; product R_f = 0.5). After 19 hours, TLC (50% hexanes in ethyl acetate; product R_f = 0.78) showed some starting material remaining. The solvent was removed under a vacuum, leaving a green flaky solid. The product was used without further purification. MS *m/z*: [M^+] calcd 216; found 216

1,2,3,6-Tetrahydro-1-(1-napthylmethyl)-4-phenylpyridine (15). In a dry 50 mL round bottomed flask with magnetic stir bar and septa, 330 mg (1.03 mmol, 1.03 eq) of compound **7**, 1.1 mL of triethylsilane (9.5 mmol, 9.5 eq), and 0.5 mL (6.5 mmol, 6.5 eq) of trifluoroacetic acid were stirred under nitrogen atmosphere for 24 hours. The reaction was diluted with 30 mL dichloromethane, washed with 3x20 mL 1M sodium hydroxide, and dried over magnesium sulfate. A TLC plate was developed with the reaction mixture (50% hexanes in ethyl acetate, product R_f = 0.69). Automated flash chromatography was used for purification, giving white crystals. Crude yield: 23%, purified yield, 16%. MS *m/z*: [M^+] calcd 299; found 299

1-Benzyl-1,2,3,6-tetrahydro-4-phenylpyridine (16). In a dry 25 mL round bottomed flask with magnetic stir bar and septum, 140 mg (0.52 mmol, 0.52 eq) compound **6**, 0.5 mL (4.3 mmol, 4.3 eq) triethylsilane, and 0.25 mL (3.25 mmol, 3.25 eq) trifluoroacetic acid were stirred at room temperature under nitrogen for 24 hours. The mixture was diluted in 15 mL dichloromethane, washed with 2x30 mL of 1 M sodium hydroxide, and dried over magnesium sulfate. The solvent was removed under vacuum, and a TLC of the mixture was developed (50% hexanes in ethyl acetate, product $R_f = 0.55$). Automated flash chromatography (10 g SNAP Ultra column, hexanes/ethyl acetate gradient) was used for purification, giving yellow-white crystals. MS *m/z*: [M^+] calcd 249; found 249

References

(1) World Health Organization. *Global Tuberculosis Report 2017*; 2017.

(2) Zhang, Y. The Magic Bullets and Tuberculosis Drug Targets. *Annu. Rev. Pharmacol. Toxicol.* **2005**, *45* (1), 529–564. https://doi.org/10.1146/annurev.pharmtox.45.120403.100120.

(3) Chiaradia, L.; Lefebvre, C.; Parra, J.; Marcoux, J.; Burlet-Schiltz, O.; Etienne, G.; Tropis, M.; Daffé, M. Dissecting the Mycobacterial Cell Envelope and Defining the Composition of the Native Mycomembrane. *Sci. Rep.* **2017**, *7* (1). https://doi.org/10.1038/s41598-017-12718-4.

(4) Schiebel, J.; Kapilashrami, K.; Fekete, A.; Bommineni, G. R.; Schaefer, C. M.; Mueller, M. J.; Tonge, P. J.; Kisker, C. Structural Basis for the Recognition of Mycolic Acid Precursors by KasA, a Condensing Enzyme and Drug Target from *Mycobacterium Tuberculosis*. *J. Biol. Chem.* **2013**, *288* (47), 34190–34204. https://doi.org/10.1074/jbc.M113.511436.

(5) Marrakchi, H.; Lanéelle, M.-A.; Daffé, M. Mycolic Acids: Structures, Biosynthesis, and Beyond. *Chem. Biol.* **2014**, *21* (1), 67–85. https://doi.org/10.1016/j.chembiol.2013.11.011.

(6) Sullivan, T. J.; Truglio, J. J.; Boyne, M. E.; Novichenok, P.; Zhang, X.; Stratton, C. F.; Li, H.-J.; Kaur, T.; Amin, A.; Johnson, F.; et al. High Affinity InhA Inhibitors with Activity against Drug-Resistant Strains of *Mycobacterium Tuberculosis*. *ACS Chem. Biol.* **2006**, *1* (1), 43–53. https://doi.org/10.1021/cb0500042.

(7) Bommineni, G. R.; Kapilashrami, K.; Cummings, J. E.; Lu, Y.; Knudson, S. E.; Gu, C.; Walker, S. G.; Slayden, R. A.; Tonge, P. J. Thiolactomycin-Based Inhibitors of Bacterial β-Ketoacyl-ACP Synthases with in Vivo Activity. *J. Med. Chem.* **2016**, *59* (11), 5377–5390. https://doi.org/10.1021/acs.jmedchem.6b00236.

(8) Brown, A. K.; Taylor, R. C.; Bhatt, A. Platensimycin Activity against Mycobacterial B-Ketoacyl- ACP Synthases. *PLoS ONE* **2009**, *4* (7), 10.

(9) Das, M.; Sakha Ghosh, P.; Manna, K. A Review on Platensimycin: A Selective FabF Inhibitor. *Int. J. Med. Chem.* **2016**, *2016*, 1–16. https://doi.org/10.1155/2016/9706753.

(10) Bhatt, A.; Kremer, L.; Dai, A. Z.; Sacchettini, J. C.; Jacobs, W. R. Conditional Depletion of KasA, a Key Enzyme of Mycolic Acid Biosynthesis, Leads to Mycobacterial Cell Lysis. *J. Bacteriol.* **2005**, *187* (22), 7596–7606. https://doi.org/10.1128/JB.187.22.7596-7606.2005.

(11) Duan, X.; Xiang, X.; Xie, J. Crucial Components of Mycobacterium Type II Fatty Acid Biosynthesis (Fas-II) and Their Inhibitors. *FEMS Microbiol. Lett.* **2014**, *360* (2), 87–99. https://doi.org/10.1111/1574-6968.12597.

(12) Luckner, S. R.; Machutta, C. A.; Tonge, P. J.; Kisker, C. Crystal Structures of Mycobacterium Tuberculosis KasA Show Mode of Action within Cell Wall Biosynthesis and Its Inhibition by Thiolactomycin. *Struct. Lond. Engl. 1993* **2009**, *17* (7), 1004–1013. https://doi.org/10.1016/j.str.2009.04.012.

(13) Konc, J.; Lešnik, S.; Janežič, D. Modeling Enzyme-Ligand Binding in Drug Discovery. *J. Cheminformatics* **2015**, *7*. https://doi.org/10.1186/s13321-015-0096-0.

(14) Pryde, D. C.; Corless, M.; Fenwick, D. R.; Mason, H. J.; Stammen, B. C.; Stephenson, P. T.; Ellis, D.; Bachelor, D.; Gordon, D.; Barber, C. G.; et al. The Design and Discovery of Novel Amide CCR5 Antagonists. *Bioorg. Med. Chem. Lett.* **2009**, *19* (4), 1084–1088. https://doi.org/10.1016/j.bmcl.2009.01.012.
(15) Brožič, P.; Turk, S.; Adeniji, A. O.; Konc, J.; Janežič, D.; Penning, T. M.; Lanišnik Rižner, T.; Gobec, S. Selective Inhibitors of Aldo-Keto Reductases AKR1C1 and AKR1C3 Discovered by Virtual Screening of a Fragment Library. *J. Med. Chem.* **2012**, *55* (17), 7417–7424. https://doi.org/10.1021/jm300841n.
(16) Rogers, H. R.; Rogers, R. J.; Mitchell, H. L.; Whitesides, G. M. Mechanism of Formation of Grignard Reagents. Kinetics of Reaction of Substituted Aryl Bromides with Magnesium and with Tri-n-Butyltin Hydride in Ethereal Solvents. *J. Am. Chem. Soc.* **1980**, *102* (1), 231–238. https://doi.org/10.1021/ja00521a036.
(17) Knochel, P.; M. Barl, N.; Werner, V.; Sämann, C. The Halogen/Magnesium-Exchange Using IPrMgCl·LiCl and Related Exchange Reagents. *HETEROCYCLES* **2014**, *88* (2), 827. https://doi.org/10.3987/REV-13-SR(S)4.
(18) Wittig, G.; Schöllkopf, U. Zum Chemismus Der Halogen-Lithium-Austauschreaktion. *Tetrahedron* **1958**, *3* (1), 91–93. https://doi.org/10.1016/S0040-4020(01)82616-8.
(19) Schlosser, M. *Organometallics in Synthesis: A Manual*, 1. paperback ed.; Wiley: Chichester, 1996.
(20) Holland, H. L.; Morris, T. A.; Nava, P. J.; Zabic, M. A New Paradigm for Biohydroxylation by Beauveria Bassiana ATCC 7159. *Tetrahedron* **1999**, *55* (24), 7441–7460. https://doi.org/10.1016/S0040-4020(99)00393-2.
(21) Seo, H.; Katcher, M. H.; Jamison, T. F. Photoredox Activation of Carbon Dioxide for Amino Acid Synthesis in Continuous Flow. *Nat. Chem.* **2017**, *9* (5), 453–456. https://doi.org/10.1038/nchem.2690.
(22) Davies, M. W.; Shipman, M.; Tucker, J. H. R.; Walsh, T. R. Control of Pyramidal Inversion Rates by Redox Switching. *J. Am. Chem. Soc.* **2006**, *128* (44), 14260–14261. https://doi.org/10.1021/ja065325f.
(23) Cid, J. M.; Tresadern, G.; Duvey, G.; Lütjens, R.; Finn, T.; Rocher, J.-P.; Poli, S.; Vega, J. A.; de Lucas, A. I.; Matesanz, E.; et al. Discovery of 1-Butyl-3-Chloro-4-(4-Phenyl-1-Piperidinyl)-(1 *H*)-Pyridone (JNJ-40411813): A Novel Positive Allosteric Modulator of the Metabotropic Glutamate 2 Receptor. *J. Med. Chem.* **2014**, *57* (15), 6495–6512. https://doi.org/10.1021/jm500496m.
(24) Gandour, R. *Handbook of Reagents for Organic Synthesis; Oxidizing and Reducing Agents*. John Wiley and Sons, New York, NY. 2000; Vol. 63. https://doi.org/10.1021/np990739q.
(25) Doyle, M. P.; West, C. T. Silane Reductions in Acidic Media. VI. Mechanism of Organosilane Reductions of Carbonyl Compounds. Transition State Geometries of Hydride Transfer Reactions. *J. Org. Chem.* **1975**, *40* (26), 3835–3838. https://doi.org/10.1021/jo00914a004.
(26) Carson, B. E.; Parker, T. M.; Hohenstein, E. G.; Brizius, G. L.; Komorner, W.; King, R. A.; Collard, D. M.; Sherrill, C. D. Competition Between π–π and C□H/π Interactions: A Comparison of the Structural and Electronic Properties of Alkoxy-Substituted 1,8-Bis((Propyloxyphenyl)Ethynyl)Naphthalenes. *Chem. – Eur. J.* **2015**, *21* (52), 19168–19175. https://doi.org/10.1002/chem.201502363.

(27) Yuki Arakawa; Shunpei Nakajima; Ryohei Ishige; Makoto Uchimura; Sungmin Kang; Gen-ichi Konishi; Junji Watanabe. Synthesis of Diphenyl-Diacetylene-Based Nematic Liquid Crystals and Their High Birefringence Properties. *J. Mater. Chem. 22* (17), 8394. https://doi.org/10.1039/c2jm16002a, info:doi/10.1039/c2jm16002a.
(28) Hsieh, Y.-C.; Chir, J.-L.; Yang, S.-T.; Chen, S.-J.; Hu, C.-H.; Wu, A.-T. A Sugar-Aza-Crown Ether-Based Fluorescent Sensor for Cu2+ and Hg2+ Ions. *Carbohydr. Res.* **2011**, *346* (7), 978–981. https://doi.org/10.1016/j.carres.2011.03.010.
(29) Guo, X.; Bruins, A. P.; Covey, T. R. Characterization of Typical Chemical Background Interferences in Atmospheric Pressure Ionization Liquid Chromatography-Mass Spectrometry. *Rapid Commun. Mass Spectrom.* **2006**, *20* (20), 3145–3150. https://doi.org/10.1002/rcm.2715.

Appendix I

Materials

Reagents and Materials	***Provider***	***Purity***
1-Pyrenemethanol	TCI AMERICA	98.00%
Thionyl chloride, Reagentplus	Sigma Aldrich Corporation	99.50%
Hexane	Thermo Fisher Scientific	Pesticide Residue Analysis Grade
Ethyl acetate	Thermo Fisher Scientific	HPLC Grade
TLC plates, silica gel on glass	Aldrich	-
1,4-Dibromobenzene	Thermo Fisher Scientific	99%
n-Butyllithium, 2.2 M in hexane	Alfa Aesar	-
1-Benzyl-4-piperidone	Alfa Aesar	98%
Tetrahydrofuran	Thermo Fisher Scientific	Laboratory Grade
Ammonium chloride	Sigma Aldrich Corporation	99.50%
Magnesium sulfate, anhydrous	Thermo Fisher Scientific	Certified Powder
Diphenylacetic acid	Alfa Aesar	recrystallized
Cyclohexanone	Thermo Fisher Scientific	98%
Ethyl ether	Thermo Fisher Scientific	Laboratory Grade
Nitrogen, compressed gas	Airgas, Inc.	-
Chloroform	Sigma Aldrich Corporation	99%
Iodine	Sigma Aldrich Corporation	Certified ACS
1-Bromo-4-iodobenzene	Thermo Fisher Scientific	98%
1-Boc-4-piperidone	Alfa Aesar	99%
4-(4-Bromophenyl)-4-piperidinol	Sigma Aldrich Corporation	98%
Benzyl chloride	Thermo Fisher Scientific	99.5%
Sodium carbonate, anhydrous	Sigma Aldrich Corporation	99%
Acetonitrile, anhydrous	Thermo Fisher Scientific	99.90%
1-(Chloromethyl)naphthalene	Thermo Fisher Scientific	95%
4-(4-chlorophenyl)piperidin-4-ol	ChemBridge Corporation	95%
Magnesium turnings	Alfa Aesar	99.80%
4-Hydroxy-4-phenylpiperidine	TCI AMERICA	98%
4-[3-(Trifluoromethyl)phenyl]-4-piperidinol	Alfa Aesar	97%

Appendix II

Spectra

(1) 1-methylpyrene

MW: 216.28, *m/z* [M^+]: 216

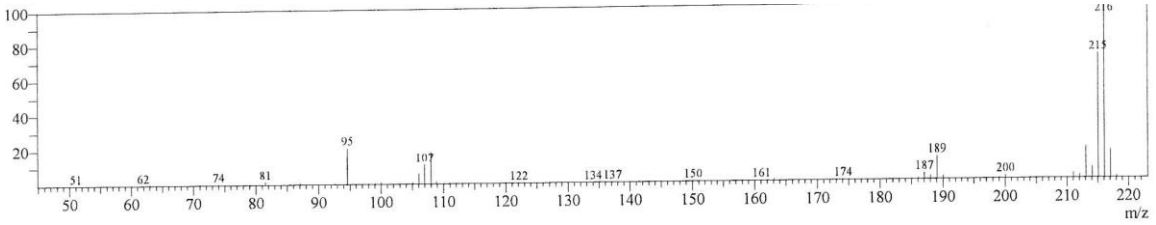

(2) 1-boc-4-phenyl-4-piperidinol

MW: 277.36, *m/z* [M^+]: 277

m/z 341, 355 due to siloxane background impurity (column bleed)[29]

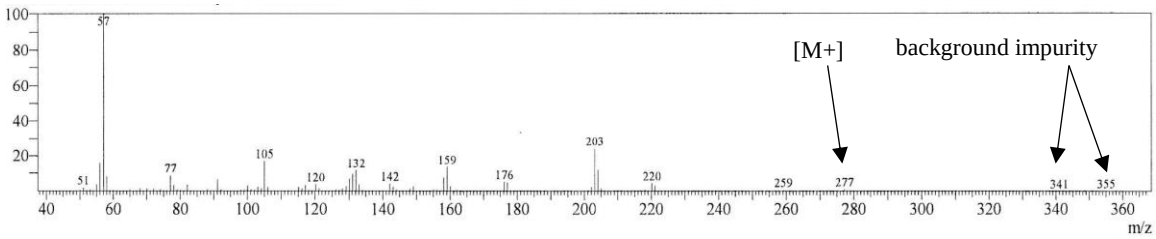

(3) 1-benzyl-4-(4-bromophenyl)-4-piperidinol

MW: 346.26, *m/z* [M^+]: 345.10

m/z 345.10 one less than MW due to loss of H from OH group

m/z 347.10 [M+2] isotope peak from Br

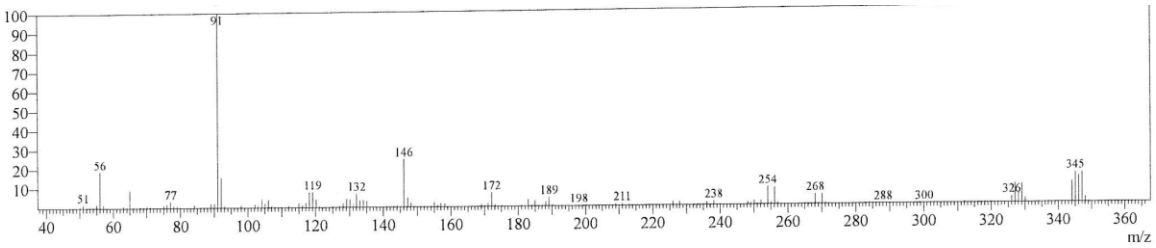

(4) 1-benzyl-4-(4-chlorophenyl)-4-piperidinol

MW: 301.81; *m/z* [M^+]: 301.20

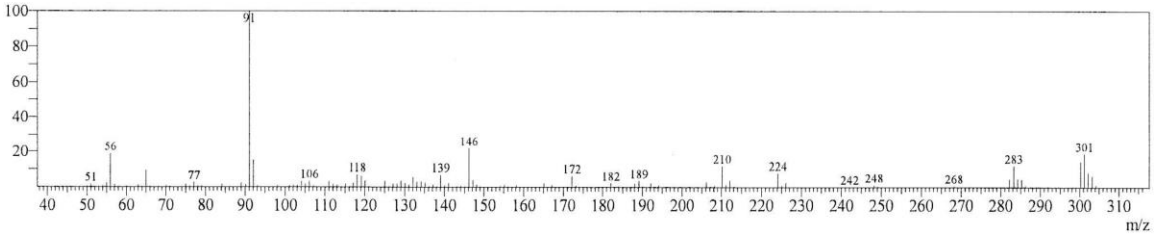

(5) 4-(4-chlorophenyl)-1-(1-naphthylmethyl)-4-piperidinol

MW: 351.87; *m/z* [M^+]: 351.15

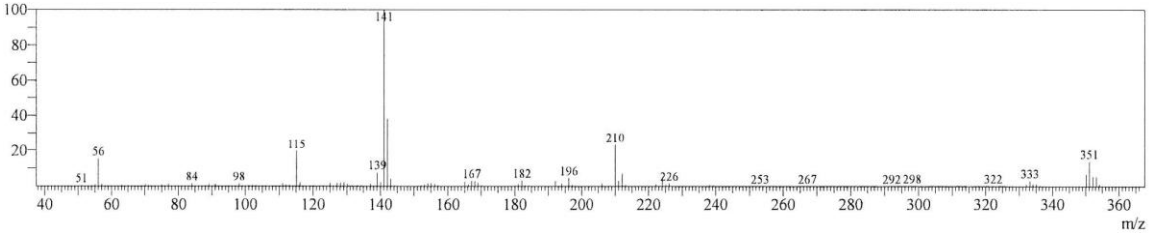

(6) 1-benzyl-4-phenyl-4-piperidinol

MW: 267.37; *m/z* [M^+]: 267.20

m/z 281 due to siloxane background impurity (column bleed)[29]

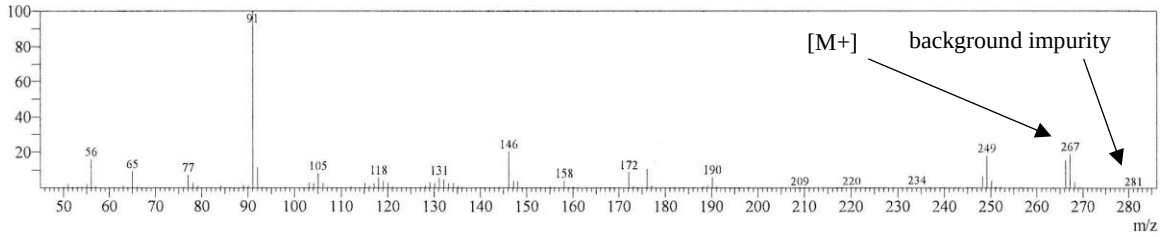

(7) 1-(1-naphthylmethyl)-4-phenyl-4-piperidinol

MW: 317.42; *m/z* [M^+]: 317.25

m/z 343, 355 due to background impurity[29]

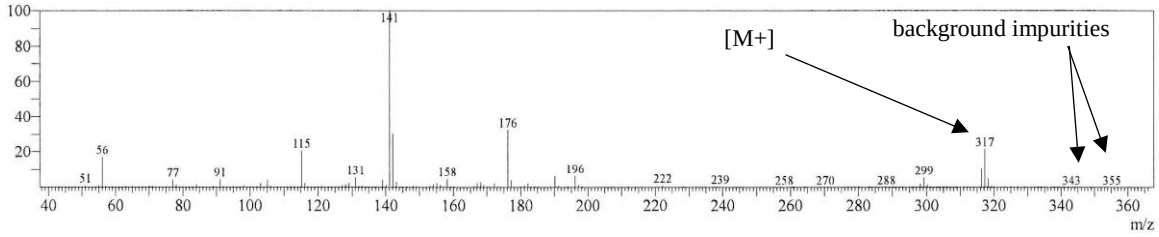

(8) 1-benzyl 4-[3-(trifluoromethyl)phenyl]-4-piperidinol

MW: 335.36; *m/z* [M^+]: 335.10

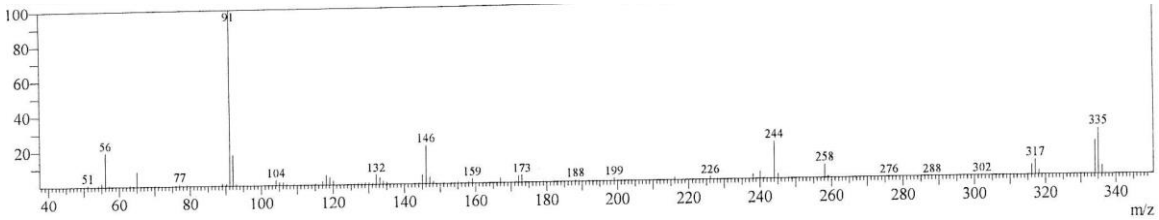

(9) 1-benzyl-1,2,3,6-tetrahydro-4-phenylpyridine

MW: 249.35; *m/z* [M^+]: 249

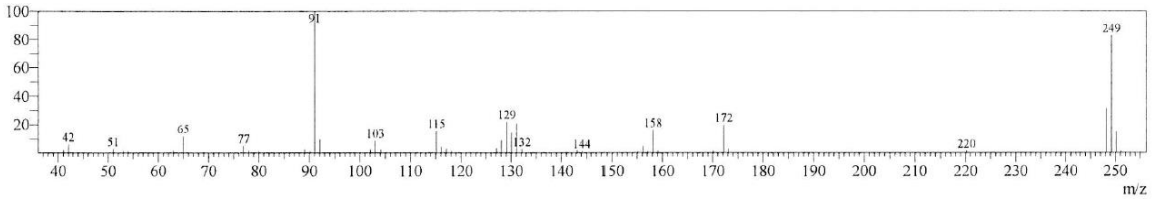

(10) 1,2,3,6-tetrahydro-1-(1-napthylmethyl)-4-phenylpyridine

MW: 299.41; *m/z* [M^+]: 299